

# Intrinsic variability of latency to first-spike

Wainrib Gilles · Thieullen Michèle ·  
Pakdaman Khashayar

Received: 31 July 2009 / Accepted: 12 March 2010 / Published online: 7 April 2010  
© Springer-Verlag 2010

**Abstract** The assessment of the variability of neuronal spike timing is fundamental to gain understanding of latency coding. Based on recent mathematical results, we investigate theoretically the impact of channel noise on latency variability. For large numbers of ion channels, we derive the asymptotic distribution of latency, together with an explicit expression for its variance. Consequences in terms of information processing are studied with Fisher information in the Morris–Lecar model. A competition between sensitivity to input and precision is responsible for favoring two distinct regimes of latencies.

**Keywords** Latency coding · Channel noise · Fisher information · Morris–Lecar model

## 1 Introduction

Neurons respond to incoming signals with action potentials. In some neurons, the latency, that is, the time separating stimulus arrival from action potential onset, can vary greatly depending on input characteristics (Hodgkin 1948). In this

way, latency may be one of the means for signal encoding in nervous systems. One key advantage of this form of neuronal coding over, say, rate coding, is the speed with which it allows information transfer and processing (Thorpe et al. 1996; Guyonneau et al. 2005). Latency coding may be ubiquitous in nervous systems, as indicated by a wide range of studies in diverse neuronal structures such as the auditory system (Furukawa and Middlebrooks 2002; Heil 2004; Chase and Young 2008), somato-sensory system (Panzeri et al. 2001; Johansson and Birznieks 2004), or the visual system (Kjaer et al. 1996; Rullen 2003) both for primary (retina gollish) and higher-level (Kiani et al. 2005; Mormann et al. 2008) functions. For efficient latency coding, as in other forms of information encoding by spike timing, the precise timing of spike generation is essential. Hence, the performance of latency coding can be limited by noise-induced fluctuations in discharge times. Quantification of this effect is crucial to discuss the validity of latency coding and its possible advantages over other forms of neural coding.

In living organisms, latency from stimulus onset may be caused by several mechanisms involving many neurons and synapses. Here, we focus our study on the properties of latency at the single neuron level. Neurons are subject to various sources of noise, both intrinsic (membrane noise) and extrinsic (synaptic noise), and many studies have been concerned with its impact on information processing. The intrinsic fluctuations in single neurons are mainly caused by ion channels, also called channel noise, the impacts of which and putative functions are intensively investigated (Schneidman et al. 1998; Shuai and Jung 2003; Rossum et al. 2003; Rowat 2007). That channel noise can introduce variability in latency has been observed in intracellular recordings of neuronal membrane potentials (Verveen and Derksen 1965). This study is partly motivated by experimental works on relative latency coding. As explained in Gollisch and Meister (2008),

---

W. Gilles (✉)  
Centre de Recherche en Epistémologie Appliquée, UMR 7656,  
Ecole Polytechnique, CNRS, Paris, France  
e-mail: gilles.wainrib@polytechnique.org

T. Michèle  
Laboratoire de Probabilités et Modèles Aléatoires (LPMA),  
UMR 7599, CNRS, Univ. Paris VI, Paris VII,  
Paris, France  
e-mail: michele.thieullen@upmc.fr

P. Khashayar  
Institut Jacques Monod (IJM), UMR 7592, CNRS, Univ. Paris VII,  
Paris VI, Paris, France  
e-mail: pakdaman@ijm.univ-paris-diderot.fr

a specific point concerning relative latencies variability is that extrinsic noise is likely to induce correlated variability between different neurons. Thus, coding with relative latencies is expected to be rather efficient to cope with external variability. These observations provide a clear motivation to study the impact of intrinsic noise. Moreover, it has been shown in [Berry et al. \(1997\)](#) for retinal cells that both variability and latency decrease with stimulation strength. However, as pointed out in [Krishna \(2002\)](#), the relationship between those two quantities has not been clearly analyzed, neither experimentally nor theoretically. Here, we provide a mathematical analysis of this issue, quantifying the impact of channel noise on discharge time variability.

Previous studies on noisy latencies have considered computations of the mean latency in the deterministic and large noise regime ([Tuckwell and Wan 2005](#)), the latter being characterized by an increase of mean latency, called “noise delay decay” ([Pankratova et al. 2005](#); [Oser and Uzuntarla 2008](#)). A detection enhancement of subthreshold pulses due to internal noise has been investigated in [Chen et al. \(2008\)](#). Here, emphasis is on the impact of channel noise, in a biophysically realistic model, for suprathreshold inputs in a regime where the mean latency is approximately constant. In [Pakdaman et al. \(2009\)](#), neuron models with channel noise are studied mathematically within the framework of fluid limit for stochastic hybrid systems: in terms of latency coding, the main contributions are to describe the asymptotic distribution of latencies and a theoretical expression for its variance. In order to understand information processing, we show that it is essential to quantify the way both the output and its variance depend on the input. Our approach is thus to combine the theoretical results of [Pakdaman et al. \(2009\)](#) with an analysis of Fisher information. Given the diversity of neuronal structures in which latency coding may take place, the mathematical analysis in [Sect. 3](#) is carried out in a broad setting so as to be valid for a wide class of conductance-based neuronal models. These theoretical results are also illustrated through the computation of latency variability in the Morris–Lecar (ML) model ([Morris and Lecar 1981](#)). The choice of this model is mainly motivated by the fact that, since the seminal article ([Rinzel and Ermentrout 1989](#)), it has become one of the classical mathematical models for investigating neuronal coding, and results obtained with this model tend to be representative of wide classes of neurons ([Izhikevich 2007](#)). This application to the Morris–Lecar model shows that Fisher information can display a  $U$ -shape, resulting from a competition between sensitivity and precision. This suggests that input bimodality, leading to both short and long latencies, may be favored in terms of information transfer.

Thus, considering conductance-based neuron models with  $N$  stochastic ion channels modeled by kinetic Markov schemes ([Sect. 2](#)), we investigate theoretically the impact of intrinsic noise on latency variability ([Sect. 3](#)). As an applica-

tion of these general mathematical results, we present their consequences in terms of information transfer ([Sect. 4](#)) with numerical illustrations based on the ML model. We finally discuss our results in [Sect. 5](#).

## 2 Neuron models with channel noise

Embedded within the neuron membrane, distributed with heterogeneous densities, ion channels enable ion transfer and their collective behavior is responsible for the generation of action potentials. They are metastable molecular devices subject to thermal noise, and their stochastic conformational changes are usually modeled by kinetic Markov schemes ([Hille 2001](#)). The model we present here is a stochastic interpretation of deterministic conductance-based neuron models with a finite number of ion channels, as introduced in [Skaugen and Walloe \(1979\)](#). Let us describe briefly the original deterministic model ( $\mathbf{D}$ ) and its stochastic interpretation ( $\mathbf{S}_N$ ). For the clarity of notations, we present the stochastic version of the three-dimensional Morris–Lecar model ([Morris and Lecar 1981](#)), which will be studied in more detail in [Sect. 4](#). The general theoretical framework can be found in [Pakdaman et al. \(2009\)](#) and analysis of [Sect. 3](#) thus holds for a wide class of stochastic conductance-based models.

*Model (D).* The membrane potential  $V$  and the proportions of open ion channels  $u_i$  for  $i = \text{K, Ca}$  satisfy the following system of differential equations ( $\mathbf{D}$ ):

$$\begin{aligned} \frac{dV}{dt} &= C^{-1} \left( I(t) - \sum_{i \in \text{Ca, K}} g_i u_i (V - V_i) - g_L (V - V_L) \right) \\ &:= f(V, u_{\text{Ca}}, u_{\text{K}}) \\ \frac{du_i}{dt} &= (1 - \alpha_i(V))u_i - u_i \beta_i(V) := b_i(V, u_i) \\ &\text{for } i = \text{Ca, K} \end{aligned}$$

where  $C$  is the membrane capacitance,  $I(t)$  is the input current,  $g_i$ , and  $V_i$  are the maximal conductances and reversal potentials, respectively, associated with ion  $i = \text{Ca, K}$ . In terms of notations, we denote by  $F = (f, b_{\text{Ca}}, b_{\text{K}})$  the vector field defining the deterministic model ( $\mathbf{D}$ ). The auxiliary functions and the parameters set used are given in [Appendix B](#). The solution of ( $\mathbf{D}$ ) will be denoted  $\mathbf{x} = (V, u_{\text{Ca}}, u_{\text{K}})$ .

The mathematical analysis in [Pakdaman et al. \(2009\)](#) provides a rigorous basis for the introduction of an associated neuron model ( $\mathbf{S}_N$ ) with stochastic ion channels, in the sense that, at the limit of infinite number of ion channels, one retrieves the deterministic model.

*Model (S<sub>N</sub>)*

- Consider a finite number  $N = N_{Ca} = N_K$  of calcium and potassium channels, and denote by  $u_{Ca}^{(N)}$  and  $u_K^{(N)}$  the proportions of open calcium and potassium channels, respectively. Denoting  $V^{(N)}$  the membrane potential, each calcium and potassium channel opens and closes with voltage-dependent opening rates  $\alpha_{Ca}(\cdot)$ ,  $\alpha_K(\cdot)$  and closing rates  $\beta_{Ca}(\cdot)$ ,  $\beta_K(\cdot)$ , functions of  $V^{(N)}$ , according to independent kinetic Markov schemes:

Closed  $\rightleftharpoons$  Open

- Voltage dynamics satisfies the following differential equation between the jumps:

$$\frac{dV^{(N)}}{dt} = f(V^{(N)}, u_{Ca}^{(N)}, u_K^{(N)}) \tag{1}$$

The solution of  $(S_N)$  will be denoted by

$$\mathbf{x}_N = (V^{(N)}, u_{Ca}^{(N)}, u_K^{(N)})$$

### 3 Theoretical analysis

We present in this section the theoretical results for the variance of the latency. Let us first describe our setting.

#### 3.1 Deterministic and stochastic latency

As an input, we consider the application of a time-dependent current  $I(t)$  such that  $I(t) = 0$  for  $t < t_0$ . Depending on the characteristics of this input, such as its amplitude and steepness for instance, action potentials may be generated. We define latency as the first-passage time for the membrane potential through an arbitrary threshold  $V_{th}$  (Fig. 1a).

Latency coding is based on the dependence of latency on input characteristics. However, we have chosen to focus on a single input feature to make a clearer presentation of both theoretical and numerical results. We point out that the mathematical results of Sect. 3.2 are valid for a general input  $I(t)$ . From now on, as an input, we consider an instantaneous current impulse, resulting in an approximately instantaneous voltage shift at  $t = t_0$ . Equivalently, starting from the equilibrium point  $\mathbf{x}^* = (V^*, u_{Ca}^*, u_K^*)$  of  $(D)$ , we impose a membrane potential shift  $V^* \rightarrow V^* + A$  at time  $t = t_0$ . Then, if  $A$  is above a threshold value  $A_{th}$ , then an action potential occurs, and the deterministic latency  $T(A)$  depends on the value of  $A$  (Fig. 1b). More precisely,  $T(A)$  is generally a decreasing function of the input amplitude  $A$  (Fig. 2).

The above deterministic setting has a direct stochastic counterpart. With the same initial conditions, we substitute the deterministic trajectory with stochastic ones, according to  $(S_N)$ , and we define in the same manner the stochastic latency

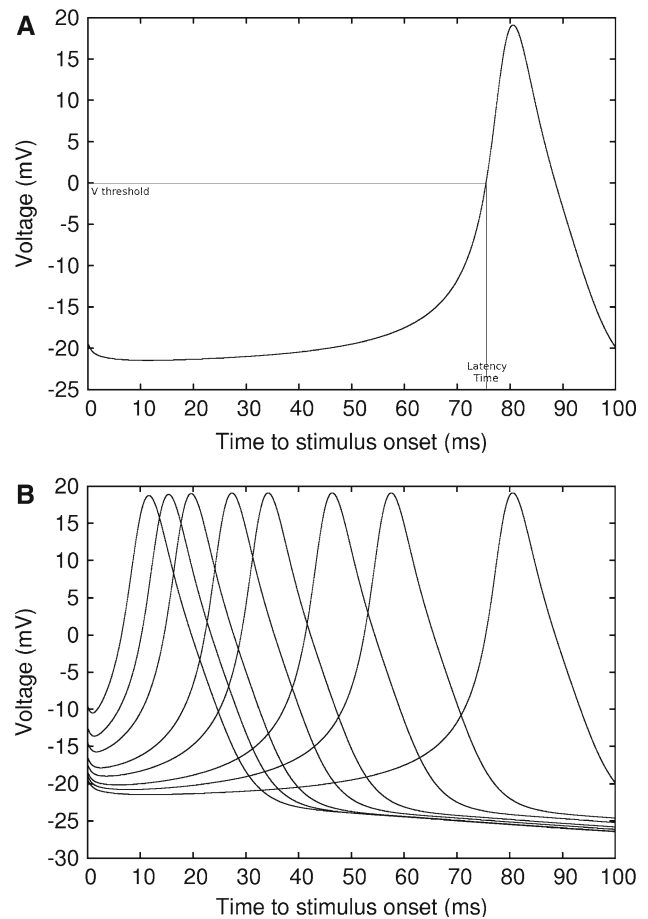


**Fig. 1** Time course of membrane potential  $V$  of the ML model for a suprathreshold stimulation. Latency is defined as the time separating stimulus onset from the voltage crossing  $V_{threshold}$ . **a** Definition of latency as the first-passage time through a threshold  $V_{th}$ . In **b**, several time courses of  $V$  corresponding to different values of  $A$  are shown

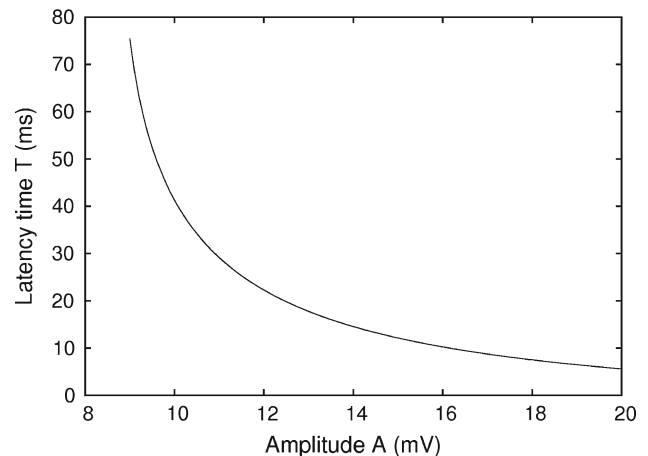


**Fig. 2** Latency versus Stimulus amplitude for the ML model. Amplitudes are suprathreshold ( $A > A_{th}$ )

$T_N(A)$ . Illustrative sample waveforms are shown in Fig. 3: trajectories starting from the same initial point lead to different latencies. One can readily observe that the variability

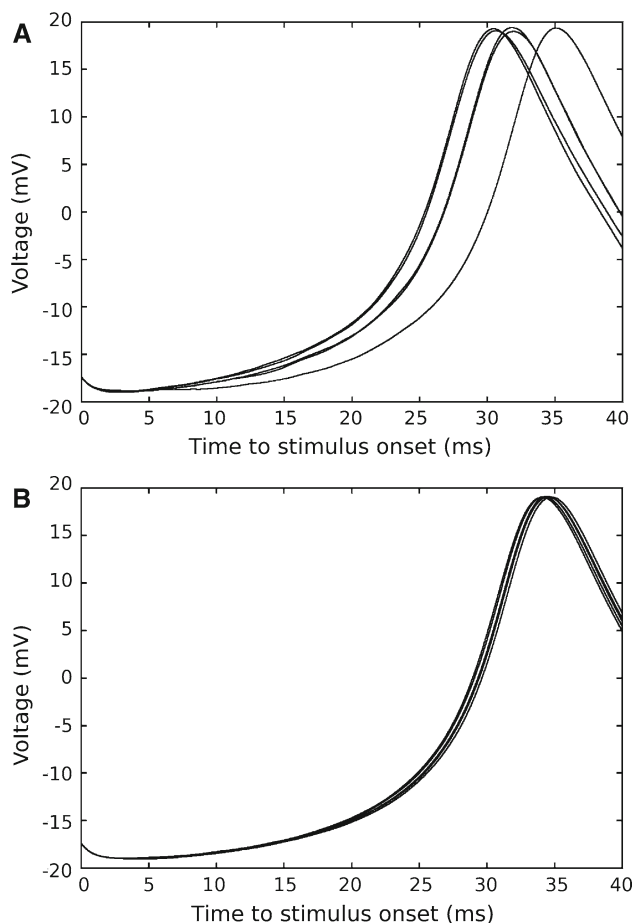


**Fig. 3** Sample trajectories of the stochastic ML model leading to random latencies. **a**  $N = 1,000$ . **b**  $N = 10,000$

seems higher in Fig. 3a where  $N = 1,000$  than in Fig. 3b where  $N = 10,000$ . One also expects this variability to depend on the amplitude  $A$ . These early observations will be made more precise in the following sections.

Stationary fluctuations of neuronal state may be considered as an additional source of latency variability, since initial values at the stimulus onset  $t = t_0$  change from trial to trial. A way to study this effect is to draw random initial values according to a random initial distribution for the stochastic process  $(S_N)$ , instead of starting from the equilibrium point. Both the impact of initial value randomness and fluctuations along the trajectory can be studied separately, and gathered by the following equality:

$$P_N(t) = \int_{R^d} P_N(t|x)\mu_N(dx) \tag{2}$$

where  $t > 0$ ,  $P_N(t) = \mathbf{P}[T_N \in [t, t + dt]]$ ,  $P_N(t|x) = \mathbf{P}[T_N \in [t, t + dt]|X^* = x]$ , and  $\mu_N(dx)$  the random initial distribution of the stochastic process  $(S_N)$ . Such a decomposition has been introduced for instance in Tanabe and Pakdaman (2001) and in Lansky and Musila (1991) with a focus

on the impact of random initial condition on the first passage time for a Stein’s neuron model. We will revert to this question after the presentation of the mathematical results for the setting where the initial conditions are fixed at the equilibrium point.

### 3.2 Mathematical results

In this section, we summarize key mathematical results for the theoretical analysis of the impact of channel noise on latency variability.

Let  $\mathbf{x}_N$  and  $\mathbf{x}$  being the respective solutions of  $(S_N)$  and  $(D)$ . If  $N \rightarrow \infty$ , then  $\mathbf{x}_N$  converges to  $\mathbf{x}$  in probability over finite time intervals. The fluctuations around the deterministic limit are then described with a Central Limit Theorem (CLT), which extends to a CLT for the hitting times. Let us present the main results in the following:

**Theorem (Pakdaman et al. 2009)** *If  $f, \alpha_i, \beta_i$  are  $C^1$  and if the deterministic solution of  $(D)$  is bounded, then, for appropriate initial conditions:*

1. *Law of large numbers: For all  $T > 0$  fixed and all  $\delta > 0$ , define  $p_N(T, \delta) := \mathbf{P}[\sup_{[0, T]} |\mathbf{x}_N - \mathbf{x}| > \delta]$ . Then:*

$$\lim_{N \rightarrow \infty} p_N(T, \delta) = 0 \tag{3}$$

*More precisely, there exist constants  $B, C > 0$  such that:*

$$\limsup_{N \rightarrow \infty} \frac{1}{N} \log p_N(T, \delta) \leq -\frac{\delta e^{-BT^2}}{CT} \tag{4}$$

2. *CLT for the process: The rescaled process  $\mathbf{z}_N = \sqrt{N}(\mathbf{x}_N - \mathbf{x})$  converges in law to a inhomogeneous Ornstein–Uhlenbeck diffusion process  $\mathbf{z} = (z_V, z_{Ca}, z_K)$  satisfying:*

$$dz_V = \nabla f(\mathbf{x}(t)) \cdot \mathbf{z}(t)dt \tag{5}$$

$$dz_i = \nabla b_i(\mathbf{x}(t)) \cdot \mathbf{z}(t)dt + q_i(\mathbf{x}(t))dW_t^{(i)} \tag{6}$$

where  $q_i(\mathbf{x}) = [(1 - \alpha_i(V))u_i + u_i\beta_i(V)]^{1/2}$  and  $W_t^{(i)}$  are two standards Brownian motions, for  $i = Ca, K$ .

3. *CLT for hitting-times: Assuming  $T(A) < \infty$  and  $f(X(T(A))) > 0$ , the rescaled difference  $\pi_N(A) = \sqrt{N}(T_N(A) - T(A))$  converges in law to a Gaussian-centered random variable  $\pi(A)$ , whose variance is*

$$\sigma(A) = \mathbf{E} \left[ z_V(T(A))^2 \right] / f(\mathbf{x}(T(A)))^2 \tag{7}$$

The law of large numbers and its convergence estimate (4) are obtained using martingale theory. The CLT for the process

follows from an asymptotic expansion of the master equation, or equivalently the infinitesimal generator, and leads to the CLT for hitting-times. We provide in Appendix C some heuristics concerning the CLTs 2. and 3. and for the detailed proofs, we refer the reader to Pakdaman et al. (2009). This result will be illustrated in the next section by stochastic simulations. Moreover, formula (7) provides a decomposition of the variance  $\sigma(A)$  in terms of two distinct contributions: the variance of the  $V$ -component  $z_V$  of the fluctuation process  $\mathbf{z}$  at time  $T(A)$  on the one hand, and the slope  $dV/dt$  or  $f(\mathbf{x}(T(A)))$  at the threshold crossing point, on the other. This result is still valid with a general definition of the threshold as the first time a function  $\psi(\mathbf{x}(t))$  of the trajectory crosses 0 (with a slight modification of formula (7)).

Let us discuss, in the context of central limit approximations, the interest of the convergence estimate (4) in the law of large numbers. An interpretation of the CLT for hitting-times is that the stochastic latency  $T_N(A)$  is approximately distributed as  $T(A) + N^{-\frac{1}{2}}\pi(A)$  with  $\pi(A)$  a Gaussian-centered variable of variance  $\sigma(A)$ . One may wonder on what time scale this approximation is reasonable. Indeed, given  $N$  finite, if  $T_N(A)$  is large, then one expects that fluctuations of order  $N^{-\frac{1}{2}}$  are not the only contribution and that large fluctuations may have a non-negligible impact, which will not be estimated by a CLT. Even though large fluctuations cannot be excluded, their probability of occurrence may be very small. In this case, the central limit approximation will be considered as satisfactory. A way to tackle quantitatively this problem is to refer to point 1. of the Theorem with  $\delta = O(N^{-\frac{1}{2}})$ . Given  $N$  and  $T(A)$ , the value of  $p_N(T(A), O(N^{-\frac{1}{2}}))$  is the probability that the fluctuations remain of order  $N^{-\frac{1}{2}}$  during a time interval  $[0, T(A)]$ , and inequality (4) provides a bound to this probability. Thus, point 1. in the Theorem helps quantify the quality of the central limit approximation.

The computation of  $\mathbf{E}[z_V(T(A))^2]$  can be done by at least two methods. The first one is based on the moment equations for the linear stochastic differential equations (5–6) (cf. Pakdaman et al. 2009). The other one is based on the resolvent matrix  $R(t)$  of the linear system  $\dot{\mathbf{y}} = J(t)\mathbf{y}$ , where  $J(t) = \nabla F(\mathbf{x}(t))$  is the Jacobian matrix around the deterministic limit  $\mathbf{x}(t)$ . The components of the matrix  $R$  will be denoted by  $R_{x,y}$  with  $x, y \in \{V, u_i\}$ . Here,  $R$  actually depends on the initial shift  $A$  through  $\mathbf{x}(t)$ .

**Corollary** *Introducing the matrices*

$$Q(t) := \text{diag}(0, q_{Ca}(\mathbf{x}(t)), q_K(\mathbf{x}(t))) \tag{8}$$

$$\Theta(t) := R^{-1}(t)Q(t) \tag{9}$$

$$\Omega(t) := R(t) \left( \int_0^t \Theta(s)\Theta^*(s)ds \right) R(t)^* \tag{10}$$

the variance  $\sigma(A)$  is given by:

$$\sigma(A) = \frac{\Omega_{V,V}(T(A))}{f(\mathbf{x}(T(A)))^2} \tag{11}$$

where  $\Omega_{x,y}$  is the  $x, y$ -component of  $\Omega$  for  $x, y \in \{V, u_i\}$ .

This result can be proved as follows. Let us rewrite the above equations (5–6) as

$$d\mathbf{z}_t = J(t)\mathbf{z}_t dt + Q(t)d\mathbf{w}_t \tag{12}$$

where  $\mathbf{w}_t$  is a standard multi-dimensional brownian motion. Then, the covariance matrix  $C(t, t') = \mathbf{E}(\mathbf{z}(t)\mathbf{z}(t')^*)$ , with  $\mathbf{z}^*$  denoting the transpose of  $\mathbf{z}$ , is obtained by the method of variation of the constant: indeed,

$$\mathbf{z}(t) = R(t) \int_0^t R^{-1}(s)Q(s)d\mathbf{w}_s \tag{13}$$

implies

$$C(t, t') = R(t)H(t \wedge t')R(t')^* \tag{14}$$

$$H(t) = \int_0^t R^{-1}(s)Q(s)Q(s)^*R^{-1}(s)^* ds \tag{15}$$

In order to conclude the proof, we write

$$\mathbf{E}[z_V(T(A))^2] = C_{V,V}(T(A), T(A)) \tag{16}$$

$$= \Omega_{V,V}(T(A)) \tag{17}$$

and apply formula (7).

With a similar approach, one can obtain from the resolvent matrix  $R$  the derivative  $T'(A)$ , which has an interpretation in terms of sensitivity to input (Sect. 4):

$$T'(A) = -\frac{R_{V,V}(T(A))}{f(\mathbf{x}(T(A)))} \tag{18}$$

The formulae for  $\sigma(A)$  and  $T'(A)$  in terms of the resolvent  $R(t)$  are semi-analytical, in the sense that one needs to integrate numerically the nonlinear system (D) to find  $R(t)$ . The numerical computation of  $\sigma(A)$  is thus deterministic.

At this stage, let us go back to the question of random initial conditions. The CLT described above provides a Gaussian approximation for the stationary distribution  $\mu_N(dx)$  appearing in (2). The latency  $T_N(A)$  with fixed initial conditions can also be approximated by a Gaussian distribution, and the law of the latency with random initial conditions is given by (2). This approach of gathering initial state variability and trajectory fluctuations has been used in Rossum (2001) to study the impact of several sources of noise on latency variability with integrate-and-fire neuron models. Suppose that the initial value  $\mathbf{x}(0)$  is distributed according to a given probability measure  $\mu_0(dx)$  on  $D = \mathbf{R} \times [0, 1]^2$ . A voltage shift  $V(0) \rightarrow V(0) + A$  is applied at  $t = 0$ .



In this case, the expectation and the total variance of the latency  $T_N(A, \mu_0)$  can be expressed as

$$\mathbf{E}(T_N(A, \mu_0)) = \int_D \mu_0(d\mathbf{x}) \mathbf{E}_{\mathbf{x}}(T_N(A)) \quad (19)$$

$$\text{Var}(T_N(A, \mu_0)) = \int_D \mu_0(d\mathbf{x}) \text{Var}_{\mathbf{x}}(T_N(A)) \quad (20)$$

where  $\mathbf{E}_{\mathbf{x}}$  and  $\text{Var}_{\mathbf{x}}$  are, respectively, the conditional expectation and variance, knowing the initial value  $\mathbf{x}(0) = \mathbf{x}$ . When  $N \rightarrow \infty$ , the expectation  $\mathbf{E}(T_N(A, \mu_0))$  converges to

$$T(A, \mu_0) := \int_D \mu_0(d\mathbf{x}) T(\mathbf{x}, A)$$

where  $T(\mathbf{x}, A)$  is the deterministic latency associated with an initial value  $\mathbf{x}(0) = \mathbf{x}$  and a voltage shift  $A$ . Assuming that  $\mu_0$  is centered (symmetric) around the equilibrium point  $\mathbf{x}^*$  with a small variance  $\text{Var}(\mu_0) = \epsilon \ll 1$ , one can express the limit  $T(A, \mu_0)$  as

$$T(A, \mu_0) = T(A) + \frac{\epsilon}{2} \partial_{\mathbf{xx}} T(\mathbf{x}^*, A) + o(\epsilon) \quad (21)$$

With the same approach, when  $N \rightarrow \infty$ , the variance is asymptotically equivalent to:

$$\text{Var}(T_N(A, \mu_0)) \sim \frac{1}{N} \int_D \mu_0(d\mathbf{x}) h(\mathbf{x}, A)$$

where  $h(\mathbf{x}, A) := \lim_{N \rightarrow \infty} N \mathbf{E}_{\mathbf{x}} \left[ (T_N(A) - T(\mathbf{x}, A))^2 \right]$ . In particular, if the variance  $\text{Var}(\mu_0)$  is equivalent to  $N^{-1} \sigma_0$ , as expected for the stationary fluctuations, then the corrective term is of order  $N^{-2}$  as follows:

$$\begin{aligned} \text{Var}(T_N(A, \mu_0)) &\sim \frac{1}{N} \sigma(A) \\ &+ \frac{1}{2N^2} \sigma_0 \partial_{\mathbf{xx}} h(\mathbf{x}^*, A) + o\left(\frac{1}{N^2}\right) \end{aligned}$$

We conclude that the variance of the latency still behaves asymptotically as  $N^{-1}$ , taking into account the stationary fluctuations as an initial distribution. The corrective term coming from these fluctuations in the initial data is of order  $N^{-2}$  and its impact on the total variance depends on the convexity properties of the function  $h(\cdot, A)$ .

In the next section, we focus our study on the impact of channel noise-induced trajectory fluctuations, not only on variability but also in terms of information transfer.

#### 4 Latency variability and information in the stochastic Morris–Lecar model

As shown in Fig. 2, given an amplitude, one can know the latency and conversely, from the observation of latency one

can derive the stimulus amplitude. This property, essential for latency coding, is valid in the deterministic model in the absence of any source of variability. Taking into account channel noise changes the situation because repeated presentation of the same amplitude will no longer lead to a unique latency, but to different values that change randomly from trial to trial. The challenge is to estimate the stimulus amplitude from the observation of a single latency, knowing that this quantity is subject to noise-induced variability. From an estimate of the latency distribution (Sect. 4.1), one way to accomplish this is through maximum likelihood leading to an estimation of the corresponding Fisher information, which quantifies the maximal information an ideal observer can obtain about the input knowing the output (Sect. 4.2).

##### 4.1 Latency time for the stochastic Morris–Lecar model

In order to quantify the impact of channel noise on latency in the three-dimensional Morris–Lecar model, we apply in this section, the previous theoretical results and compare the results with stochastic simulations. We have selected this model because it is considered to be the representative mathematical model for class I neuronal models in Hodgkin's classification. We remind that neurons of this class can have very long latencies. In this model, these can be even arbitrarily long. This is illustrated through the computation of the latency for a suprathreshold instantaneous pulsatile stimulus applied to a deterministic Morris–Lecar model at rest. Figure 2 shows stimulus amplitude versus latency.

Using a modified Gillespie algorithm (Gillespie 1977; Chow and White 1996), we simulate stochastic trajectories of  $(\mathbf{S}_N)$  and obtain empirical distributions for the random variable  $T_N(A)$  for different values of  $N \in \{10^3, 10^4, 10^5, 10^6\}$  and  $A$  (Fig. 4).

Confirming the theoretical analysis of Sect. 3.2, these simulations show that as  $N$  increases the law of  $T_N(A)$  becomes closer to a Gaussian (Fig. 4) centered around  $T(A)$  (Fig. 5a) and with a variance  $\sigma_N(A)$  proportional to  $N^{-1}$  (Fig. 5b). Figure 4 also illustrates that the convergence to the Gaussian distribution is faster when the stimulation is far from threshold. The dependence of the rescaled variance  $\tilde{\sigma}_N(A) := N \sigma_N(A)$  upon  $A$  is nontrivial, and we show in Fig. 6 the logarithm of the rescaled variance  $\tilde{\sigma}_N(A)$  as a function of the logarithm of the latency  $T(A)$ , both with stochastic simulations and with theoretical results for  $\sigma(A)$  obtained in Sect. 3.2, which are in very good agreement.

##### 4.2 Information transfer

Given an observation  $t_{\text{obs}}$  of the latency  $T_N(A)$  (output), a measure of the information about the amplitude shift  $A$  (input) can be estimated through Fisher information, which can be computed using the maximum likelihood

**Fig. 4** Distribution of latencies for different values of amplitude  $A$  and number of ion channels  $N$  for the stochastic Morris–Lecar model. Bars: simulation histogram. Lines: Gaussian fit.  
**a**  $A = 12$  mV,  $N = 1,000$ .  
**b**  $A = 16$  mV,  $N = 1,000$ .  
**c**  $A = 12$  mV,  $N = 10,000$ .  
**d**  $A = 16$  mV,  $N = 10,000$ .  
 For each  $A$ , the value of  $N$  times the variance is approximately constant. Histograms were made with 10,000 runs

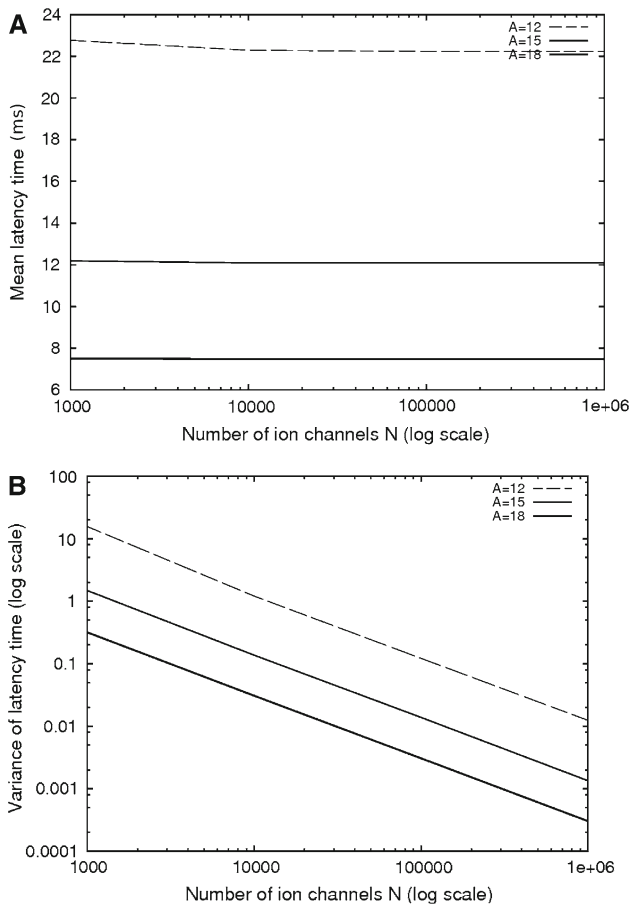
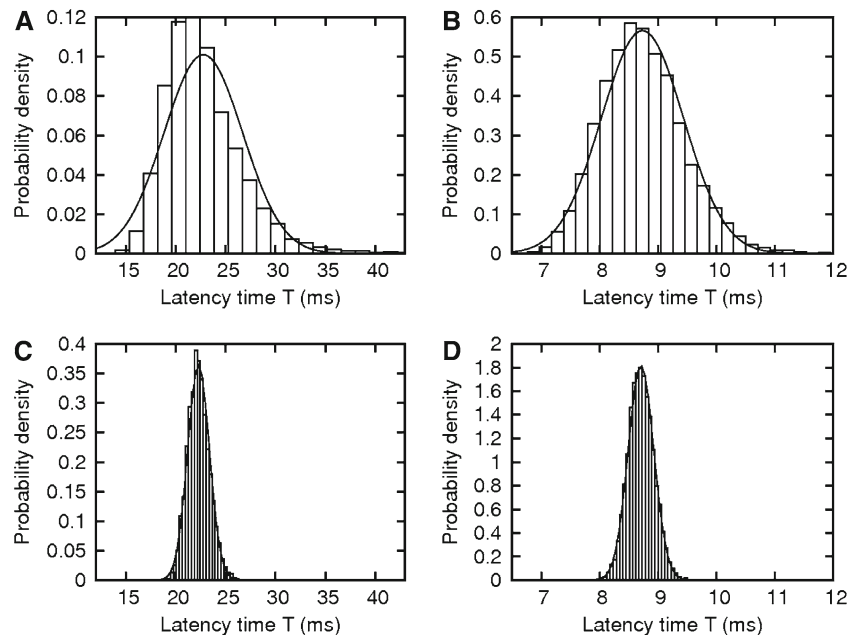


**Fig. 5** Mean and variance of latency as a function of  $N$  for different values of  $A$  from stochastic simulation. **a** mean. **b** variance. Simulations were made with 10,000 runs

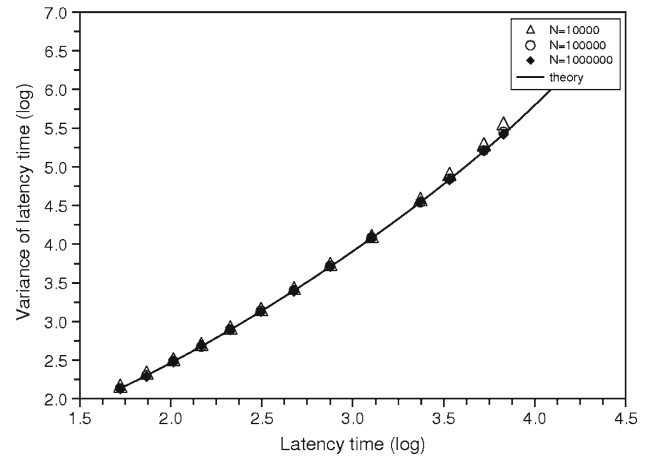


**Fig. 6** Comparison between simulations and theory for the stochastic ML model. Rescaled variance  $\tilde{\sigma}_N(A)$  (log) versus mean latency (log) by stochastic simulation for  $N = 1,000$  (up triangle),  $N = 10,000$  (circle),  $N = 1,00,000$  (filled diamond). Each point corresponds to 10,000 simulation runs. Black line: theoretical result. The points are visually indistinguishable at low latencies

principle. Here,  $T_N(A)$  is a random variable, and as shown in Sect. 3.2 its distribution can be approximated for  $N$  sufficiently large by a Gaussian distribution  $\rho_{m,v^2}(x) = (2\pi)^{-1/2}v^{-1} \exp(-(x - m)^2/(2v^2))$  with mean  $m = T(A)$  and variance  $v^2 = N^{-1}\sigma(A)$ . The idea is to maximize for  $A$  the log-likelihood

$$l_N(A|t_{\text{obs}}) = \log(\rho_{T(A), N^{-1}\sigma(A)}(t_{\text{obs}})) \tag{22}$$

Then, denoting by  $A_N^*(t_{\text{obs}})$  the maximizing value of  $A$ , we compute Fisher information as

$$I_N(t_{\text{obs}}) = \left\langle -\frac{\partial^2 l_N(A|t_{\text{obs}})}{\partial A^2} \right\rangle = -\frac{\partial^2 l_N(A|t_{\text{obs}})}{\partial A^2} \Big|_{A=A_N^*(t_{\text{obs}})}$$

As shown in Appendix A, an asymptotic expansion of Fisher information for  $N$  large yields:

$$I_N(t_{\text{obs}}) = \frac{T'^2}{\sigma} N + O(1) \tag{23}$$

where  $\sigma, T'$  are evaluated at the maximum of likelihood:

$$A_N^*(t_{\text{obs}}) = T^{(-1)}(t_{\text{obs}}) + O(1/N) \tag{24}$$

where  $T^{(-1)}$  is the inverse function of  $T$ . It is then possible to express Fisher information at the leading order using formula (11) for  $\sigma$  and formula (18) for  $T'$  as shown in Sect. 3.2. Hence, to compute this leading order term, one only needs to integrate numerically the differential equations of the deterministic model (D) given an initial shift  $A$  and to find the resolvent  $R(t)$  associated with this deterministic trajectory. In particular, no stochastic simulation is required. The interest of the mathematical results of Sect. 3.2 in terms of Fisher information analysis is thus twofold: a rigorous justification of the Gaussian approximation, which is a necessary step to estimate Fisher Information, and a semi-analytical formula for the  $\sigma(A)$  and  $T'(A)$  in terms of the resolvent, exempting Monte–Carlo simulations. The numerical results for Fisher information are displayed in Fig. 7 for different values of  $N$ , as a function of  $T(A) = t_{\text{obs}}$  (the value of  $A$  corresponding to a value of  $T(A) = t_{\text{obs}}$  can be obtained from Fig. 2). We remark that Fisher information is not constant for all latencies, nor equivalently for all inputs  $A$ , and displays a minimum. The existence of such a minimum ensures the ability to transfer a minimal quantity of information. The dependence of this minimum on the number of ion channels is shown in Fig. 7c. Moreover, with a  $U$ -shaped information, two unexpected situations may arise:

1. transfer more information with longer latencies;
2. if neurons  $i, j$  have  $N_i < N_j$  ion channels, then for appropriate inputs  $A_i$  and  $A_j$ , Fisher information  $I_{N_i}(T(A_i))$  may be higher than  $I_{N_j}(T(A_j))$ .

We understand the existence of a minimum in terms of a competition between precision and sensitivity as follows. Let us introduce the concept of sensitivity  $\eta(A) = T'(A)^2$ : if  $\eta(A)$  is large, then a small change of the input  $A$  will result in a large change of the output  $T(A)$ . For small  $A$  (large latencies  $T(A)$ ), precision is low due to a large variance  $N^{-1}\sigma(A)$  but sensitivity is large. On the other hand, for large

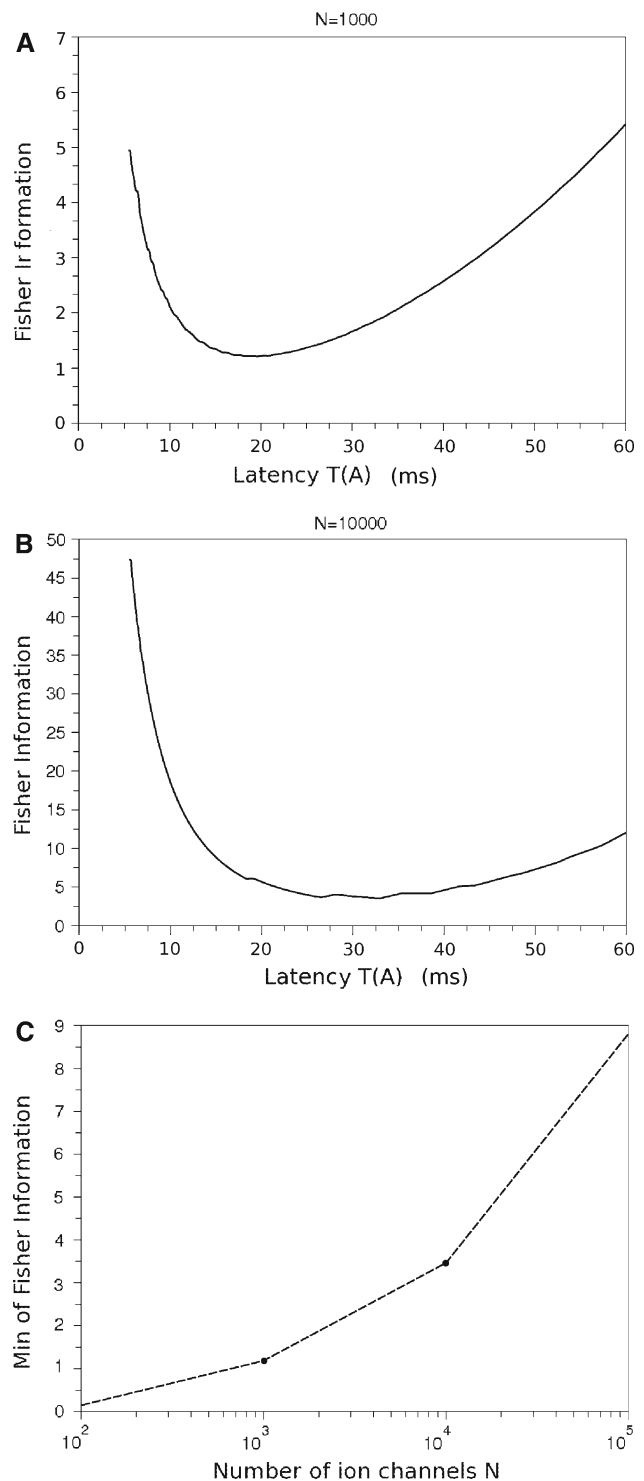


**Fig. 7** **a, b** Fisher information  $I_N$  as a function of latency  $T(A) = t_{\text{obs}}$  for different values of  $N$ . **a**  $N = 1,000$ . **b**  $N = 10,000$ . **c** Minimum of Fisher information as a function of  $N$  (log scale). Line is guide for the eye

$A$  (small latencies  $T(A)$ ), precision is high due to a small variance  $N^{-1}\sigma(A)$  but sensitivity is small. Then, depending on the precise scaling relationships between  $T(A)$ ,  $\sigma(A)$  and  $A$ , three results are *a priori* possible: information is favored



either by small  $A$ , either by large  $A$  or by intermediate  $A$  resulting from a trade-off between sensitivity and precision. This explanation is confirmed by the leading order term of Fisher information:

$$C(A) = \frac{\eta(A)}{\sigma(A)} \quad (25)$$

In the above formula, the factor  $\eta/\sigma$  corresponds to the trade-off between sensitivity and precision.

#### 4.3 Further remarks

##### 4.3.1 Impact of stimulation shape

In our study, we have considered so far an instantaneous shift of the membrane potential as an approximation of a Dirac input current. Considering a step function  $I(t) = A\mathbf{1}_{t \in [0, \tau]}$  as the input current, this approximation is justified when  $\tau$  is small compared to the expected latency. Indeed, in this case, the variability acquired during the time interval  $[0, \tau]$  is negligible compared to the variability acquired until threshold crossing. However, when  $\tau$  is not small compared to the expected latency, then the previous approximation is not valid anymore and a more refined analysis is required.

We point out that the general theoretical framework introduced in this article covers this setting of a time-dependent input. It is interesting to distinguish two cases. First if  $\tau$  is larger than the expected latency, for instance if  $\tau = +\infty$ , then one can recover the previous approximation provided the membrane potential time constant is small enough: in this case, the first phase of the trajectory can be considered as a quasi-instantaneous voltage shift. As shown in Fig. 8a and b, the dependence of the latency on the input amplitude and the relationship between the latency and the variance share similar features with the case of an instantaneous voltage shift studied previously.

The second case is when  $\tau$  is smaller than the expected latency, and of course the previous remark applies, but in this case the parameter  $\tau$  plays an explicit role since the expected latency will depend on the value of  $A$  and  $\tau$ . We present here some result concerning this setting. The first numerical observation shown in Fig. 9a is that the deterministic latency can be obtained as a strictly decreasing function of the product  $A\tau$ , when  $\tau$  is small enough. This strict monotony is essential in terms of coding. Moreover, there exists many combinations of parameters  $A$  and  $\tau$  leading to the same expected latency, and one may wonder which one minimizes the variability. In other words, is latency more precise if the stimulation is short and intense or long and weak (for a given product  $A\tau$ )? In order to address this question, we have run Monte-Carlo simulations of the stochastic model with  $N = 10,000$  ion channels for many values of  $A$  and  $\tau$ . Using the theoretical results of previous section, we have also computed numerically

(without stochastic simulations) the same quantities and the results are shown in Fig. 9b and c, where the variance is plotted against the expected latency for different values of  $\tau$ . We summarize here the three key observations resulting from this analysis:

1. A discontinuity of the relationship between the variance and the expected latency time at the end of the stimulation.
2. For latencies slightly higher than the end of the stimulation, the variance displays a local minimum.
3. For a given value of the expected latency or equivalently of the product  $A\tau$ , the variance is smaller when the stimulation is longer.

From formula (7), we provide a straightforward explanation of point 1: the denominator, which is the slope of  $V$  at threshold crossing, is much higher when the stimulation is on than after the end of the stimulation (indeed the slope is given by  $f(V, m, n) + I(t)$ ). This explains why the variance is much lower before the end of the stimulation. Having in mind the results of Sect. 4.2 about information transfer, we remark that this regime of short latency, even though very interesting in terms of precision, has a very low sensitivity, meaning that a small change in the product  $A\tau$  will result in a very small change in latency, which is not very advantageous in terms of information coding. Concerning point 2 and 3, an elementary analysis on a noisy leaky integrate-and-fire model shows that these observations are not present in such a modeling framework. These effects may be attributed either to the nonlinearities, or to the multiplicative character of the noise or to the higher dimension of the ML model (and of course to a combination of these factors). It seems that, due to the existence of other variables  $u_{Ca}$  and  $u_K$ , the value of the slope at threshold crossing is not only determined by the value of  $I(t)$  at the crossing time. The plot of this slope as a function of the latency in Fig. 9d provides an explanation for point 2. The value of the slope of  $V$  at the crossing time depends on the value of  $V$  as well as  $u_{Ca}$  and  $u_K$  at the end of the stimulation.

Furthermore, motivated by the question of an optimization, over the stimulus shape, of the variance for a given expected latency, we have also tested an alpha function for the stimulation shape. The results suggest that the variance is lower than with a step function, for a given value of the expected latency. The question of the optimal stimulation shape is a topic for future research, and the above analysis suggests that a important point is to understand how the slope at crossing depends on the stimulation shape.

##### 4.3.2 Impact of initial fluctuations

In line with the previous analysis, we investigate here the impact of random initial conditions, with a step current as a

**Fig. 8** Properties of the latency in response to a Heaviside current  $A\mathbf{1}_{t>0}$ . **a** Latency time versus stimulus amplitude displaying a strictly decreasing behavior, as in Fig. 2. **b** Rescaled variance of latency (log scale) versus deterministic latency

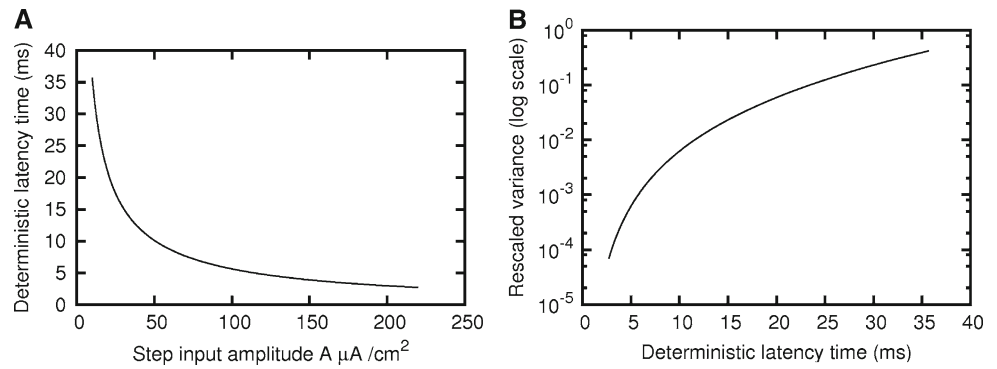
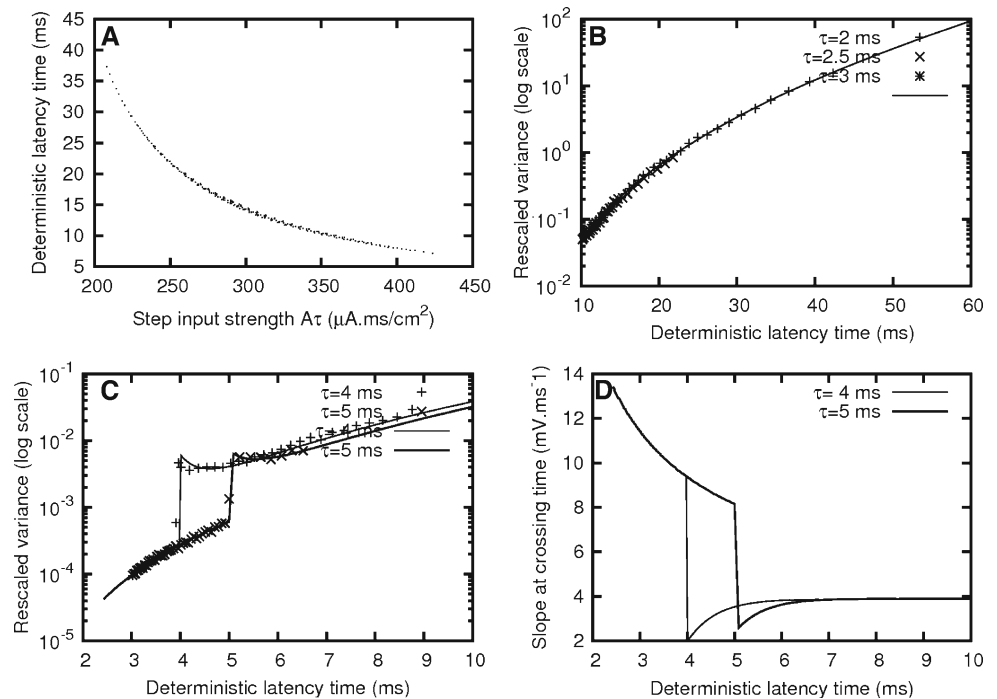


**Fig. 9** Properties of the latency in response to a step current  $A\mathbf{1}_{0<t<\tau}$ , with  $N = 10,000$ . **a** Deterministic latency versus the stimulus strength defined as  $A\tau$ , with  $A \in [100 \mu\text{A}/\text{cm}^2, 200 \mu\text{A}/\text{cm}^2]$  and  $\tau \in [2 \text{ ms}, 5 \text{ ms}]$ . **b, c** Rescaled variance of latency (log scale) versus deterministic latency. Crosses: Monte-Carlo simulation with  $10^4$  runs. Line: theory. **d** Slope of the membrane potential at crossing time versus latency



stimulation. More precisely, we start at the equilibrium point  $\mathbf{x}^*$  at time  $t = 0$  and wait for a time  $t_0$  before applying the stimulation, so that  $I(t) = A\mathbf{1}_{t_0 < t < t_0 + \tau}$ . Thus, between  $t = 0$  and  $t = t_0$ , the system is expected to converge to its stationary behavior, characterized by Gaussian fluctuations of order  $N^{-1/2}$ . In Fig. 10b, the variance for  $N = 500$  is twice the variance for  $N = 1,000$ , which is consistent with the expected  $1/N$  behavior of the variance as theoretically discussed at the end of Sect. 3. We further observe that the average latency is higher for  $N = 1,000$  than for  $N = 500$  (cf. Fig. 10a), which can be explained by the noise-induced voltage shift displayed in Fig. 10c.

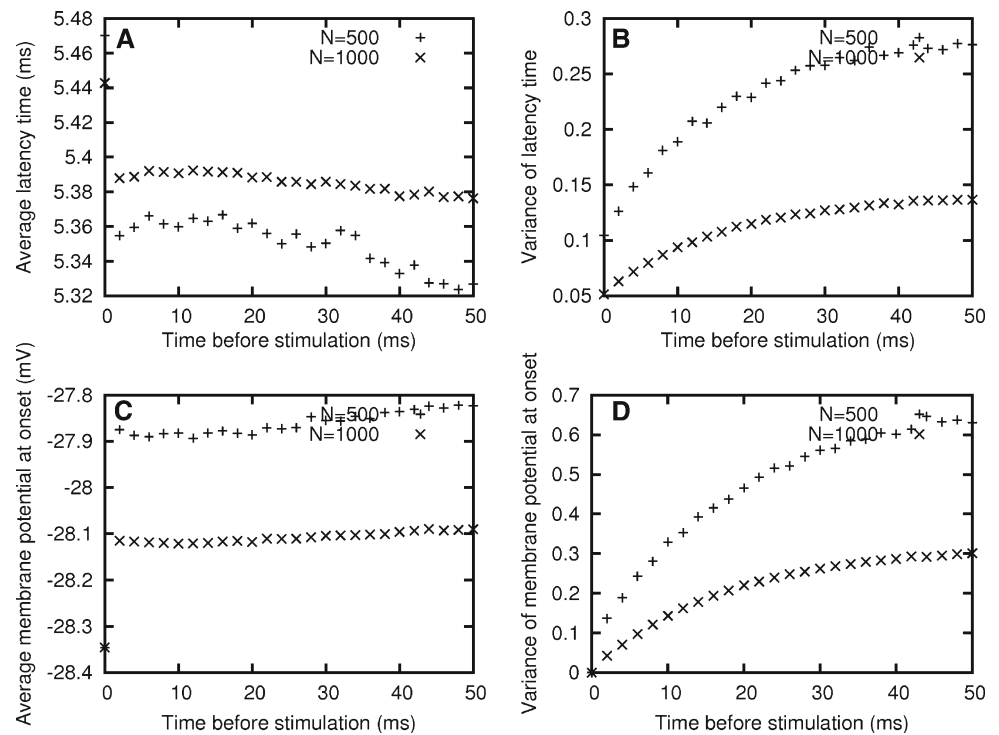
## 5 Discussion

In order to summarize, we have investigated the impact of channel noise on latency coding with a modeling approach

based on the stochastic interpretation of conductance-based models. We have shown how mathematical results of Pakdaman et al. (2009) for stochastic hybrid systems (also called piecewise-deterministic Markov processes) provide a theoretical basis for the following properties, as observed in stochastic simulation: (i) asymptotic Gaussian distributions of latencies when  $N \rightarrow \infty$ ; (ii)  $N^{-1/2}$  scaling of the standard deviation; and (iii) nontrivial variance dependence on latency, with high variance regime for near subthreshold stimulation. The theoretical analysis remains valid for other types of stimulations.

Moreover, it is possible to estimate, from Fig. 6, the number of ion channels required to produce a given variance  $\mathbf{E}[(T_N(A) - T(A))^2] \approx N^{-1}\sigma(A)$  for  $N$  large. For instance, for a specified latency  $T(A) = 30$  ms, if one requires a standard deviation of 1 ms, then one reads on Fig. 6 that  $N$  should be of order  $4 \times 10^4$ . This value can be compared to typical order of magnitudes of  $10^4$ – $10^5$  ion channels in the

**Fig. 10** Simulation results of the stochastic ML model for a delayed input current  $I(t) = A\mathbf{1}_{t_0 < t < t_0 + \tau}$ . For all the figures,  $A = 150 \mu\text{A}/\text{cm}^2$  and  $\tau = 3 \text{ ms}$ . **a** Average latency versus  $t_0$ . Latency time is shorter for lower values of  $N$ . **b** Variance of latency versus  $t_0$ . The variance increases and stabilizes with  $t_0$ , reflecting the convergence of the law of the  $x_N$  to its stationary distribution (cf. Fig. **d**). The results are consistent with the expected  $1/N$  behavior of the variance. **c** Average membrane potential at  $t = t_0$  (stimulation onset) versus  $t_0$ . This figure shows a noise-induced voltage shift, explaining Fig. **a**. **d** Variance of membrane potential at  $t = t_0$  (stimulation onset) versus  $t_0$



axonal initial segment (length 20–50  $\mu\text{m}$ , radius 0.5–2  $\mu\text{m}$  and density 100  $\mu\text{m}^{-2}$ ) deduced from the literature (Shuai and Jung 2003; Adair 2003; Arhem and Blomberg 2007). Higher sodium channel density in retinal ganglion cells have been reported (Wollner and Catterall 1986) and its interpretation is not clear (Colbert and Johnston 1996; Colbert and Pan 2002). Evidences for latency coding in these cells (Gollisch and Meister 2008) suggest an interpretation in terms of spike time precision.

The theoretical analysis provides a general method to investigate channel noise consequences in terms of neural coding with quantitative asymptotic estimates of the induced variability. As an illustration, we have exploited this method to quantify the impact of channel noise on information transfer on the Morris–Lecar neuron model, exploring a competition between sensitivity and precision. Indeed, the classical trade-off between speed of processing and precision (cf. Rossum 2001) should integrate, in the context of latency coding, the sensitivity effects. Such a competition between sensitivity and precision has also been identified in Jenison and Reale (2003) to account for an information maximum concerning latency coding in the auditory cortex. In our setting, we have shown that this competition may lead to a minimum of Fisher information as a function of the input. One way to interpret this minimum is that for all inputs, information will be higher than a certain value, ensuring a transfer with a warranted quality. On the other hand, this minimum also implies two high information regimes, both for small and long latencies. This suggests that mechanisms

may exist for the generation of bimodal latencies. It turns out that bimodal latencies were experimentally recorded in olfactory neurons (Manns and Westecker 1983) and saccade latencies also display bimodal distributions (Reulen 1984). In Liberman (1978) and Ruggero (1992) the spontaneous rates (SR) in auditory nerves are shown to follow a bimodal distribution. A link between the SR, threshold and latencies have been observed: high-SR fibers and low-SR fibers do not have the same latency response properties. A computational model has been suggested (Krishna 2002 and reference therein), accounting for this effect through an interplay between SR and the shape of the non-linearity of the auditory fiber model. At the present state of latency code understanding, it is not possible to decide whether these experimental cues of bimodal latencies are related to the  $U$ -shaped information curve obtained in Sect. 4. This question may be a direction for future research.

**Acknowledgements** This study has been supported by the ANR project MANDY, Mathematical Analysis of Neuronal Dynamics, ANR-09-BLAN-0008-01. During this study, G. Wainrib, supported by a fellowship from Ecole Polytechnique, has been hosted by the Institut Jacques Monod and the Laboratoire de Probabilités et Modèles Aléatoires, and wants to thank both of them for their hospitality. The authors thank the anonymous reviewers for their insightful comments.

**Appendix A: Fisher information for large  $N$**

The aim is to find to value of  $A$  which maximizes the likelihood:

$$L_N(A|t_{\text{obs}}) = \sqrt{\frac{N}{2\pi\sigma(A)}} \exp(-N(t_{\text{obs}} - T(A))^2 / (2\sigma(A))) \quad (26)$$

The maximum likelihood is obtained by solving

$$0 = \frac{dL_N(A|t_{\text{obs}})}{dA} = \sqrt{\frac{N}{2\pi}} B(t_{\text{obs}}, A) \exp\left(\frac{-N(t_{\text{obs}} - T(A))^2}{2\sigma(A)}\right) \quad (27)$$

with

$$B(t_{\text{obs}}, A) = \frac{\sigma(A)^{-3/2}}{2} \left[ -\sigma'(A) + \frac{N}{\sigma(A)} \times \left\{ (t_{\text{obs}} - T(A))^2 \sigma'(A) + 2T'(A)\sigma(A)(t_{\text{obs}} - T(A)) \right\} \right]$$

We assume that  $T'(A) < 0$  for all  $A$ . The meaningful solution of  $B(t_{\text{obs}}, A) = 0$  (second-order polynomial in  $x = t_{\text{obs}} - T(A)$ ) is given by:

$$t_{\text{obs}} - T(A) = \frac{\sigma(A)}{2\sigma'(A)} \left( -2T'(A) + 2\sqrt{T'(A)^2 + \frac{\sigma'(A)^2}{N\sigma(A)}} \right)$$

An expansion for large  $N$  yields:

$$A^*(t_{\text{obs}}) = T^{(-1)}(t_{\text{obs}}) + \frac{1}{N} \frac{\sigma'(T^{(-1)}(t_{\text{obs}}))}{2T'(T^{(-1)}(t_{\text{obs}}))} + o(1/N) \quad (28)$$

where  $T^{(-1)}$  is the inverse function of  $T$ . Fisher information leading order term is obtained by the following equation:

$$I_N(t_{\text{obs}}) = -\frac{\partial^2 L_N / \partial A^2}{L_N} \quad (29)$$

$$= \frac{T'^2}{\sigma} N + O(1) \quad (30)$$

where all the functions are evaluated at the maximum likelihood  $A = A^*(t_{\text{obs}})$ . Note that the leading order term  $C = \frac{T'^2}{\sigma}$  can be evaluated at  $A = T^{(-1)}(t_{\text{obs}})$  because the correction term would be of order 1.

## Appendix B: Morris–Lecar model

The auxiliary functions of the Morris–Lecar model (Morris and Lecar 1981) used in the article are:

$$\alpha_{\text{Ca}}(V) = \frac{1}{2} \cosh\left(\frac{V - V_1}{2V_2}\right) \left(1 + \tanh\left(\frac{V - V_1}{V_2}\right)\right) \quad (31)$$

$$\alpha_{\text{K}}(V) = \frac{1}{2} \lambda_n \cosh\left(\frac{V - V_3}{2V_4}\right) \left(1 + \tanh\left(\frac{V - V_3}{V_4}\right)\right) \quad (32)$$

$$\beta_{\text{Ca}}(V) = \frac{1}{2} \cosh\left(\frac{V - V_1}{2V_2}\right) \left(1 - \tanh\left(\frac{V - V_1}{V_2}\right)\right) \quad (33)$$

$$\beta_{\text{K}}(V) = \frac{1}{2} \lambda_n \cosh\left(\frac{V - V_3}{2V_4}\right) \left(1 - \tanh\left(\frac{V - V_3}{V_4}\right)\right) \quad (34)$$

The values of the parameters and initial conditions used for the numerical integration and stochastic simulations are:  $V_1 = 0$  mV;  $V_2 = 15$  mV;  $V_3 = 10$  mV;  $V_4 = 10$  mV;  $g_{\text{Ca}} = 4$  mS/cm<sup>2</sup>;  $g_{\text{K}} = 8$  mS/cm<sup>2</sup>;  $g_{\text{L}} = 2$  mS/cm<sup>2</sup>;  $V_{\text{K}} = -70$  mV;  $V_{\text{L}} = -50$  mV;  $V_{\text{Ca}} = 100$  mV;  $C = 20$   $\mu$ F/cm<sup>2</sup>;  $\lambda_n = 0.1$ ;  $I = 32$   $\mu$ A/cm<sup>2</sup>;  $m^* = 0.000466$ ;  $n^* = 0.022314$ ;  $V^* = -28.346$  mV.

## Appendix C: Heuristics for the central limit theorems

For the sake of clarity, consider that there is only one type of ion channel, say potassium channel. For  $(V, u) \in \mathbf{R} \times \{0, \frac{1}{N}, \dots, 1\}$ , the law  $P_t^{(N)}(V, u)$  of the process  $\mathbf{x}_N = (V_N, u_{\text{K}}^{(N)})$  satisfies

$$\begin{aligned} \partial_t P_t^{(N)}(V, u) &= f(V, u) \partial_V P_t^{(N)}(V, u) + N(1-u) \alpha_{\text{K}}(V) \\ &\quad \times \left[ P_t^{(N)}(V, u + \frac{1}{N}) - P_t^{(N)}(V, u) \right] + Nu \\ &\quad \times \beta_{\text{K}}(V) \left[ P_t^{(N)}(V, u - \frac{1}{N}) - P_t^{(N)}(V, u) \right] \end{aligned}$$

For  $N$  large a formal expansion of the right-hand side can be obtained introduction the first and second derivatives  $\partial_u P_t^{(N)}(V, u)$  and  $\partial_{uu} P_t^{(N)}(V, u)$ :

$$\begin{aligned} \partial_t P_t^{(N)}(V, u) &= f(V, u) \partial_V P_t^{(N)}(V, u) + ((1-u) \alpha_{\text{K}}(V) \\ &\quad - u\beta) \partial_u P_t^{(N)}(V, u) + \frac{1}{2N} ((1-u) \alpha_{\text{K}}(V) \\ &\quad + u\beta) \partial_{uu} P_t^{(N)}(V, u) + \dots \end{aligned}$$

Then one recognizes a Fokker–Planck equation: The term  $(1-u) \alpha_{\text{K}}(V) - u\beta$  corresponds to the deterministic limit and the term  $(1-u) \alpha_{\text{K}}(V) + u\beta$  to the variance in the diffusion approximation. This formal argument is made rigorous in Pakdaman et al. (2009).

The CLT for hitting times (point 3) is a consequence of the CLT for the process (point 2). The proof in Pakdaman et al. (2009) is inspired from Ethier and Kurtz (1986). We present here a sketch. For  $\mathbf{x} = (V, u) \in \mathbf{R} \times [0, 1]$ , let  $\phi(\mathbf{x}) = V - V_{\text{th}}$ . Then  $\phi(\mathbf{x}(T(A))) = 0$  by continuity and one shows that  $\sqrt{N}\phi(\mathbf{x}_N(T_N(A)))$  converges to zero. Then introducing  $\mathbf{x}_N(T_N(A))$  and using the convergence of  $Z_N$  toward  $Z$ , one shows that

$$K_N := \sqrt{N}(\phi(\mathbf{x}(T(A))) - \phi(\mathbf{x}(T_N(A))))$$

converges in law to

$$\nabla\phi(\mathbf{x}(T(A))) Z(T(A))$$

As  $K_N$  is asymptotic to

$$-\nabla\phi(\mathbf{x}(T(A))) f(\mathbf{x}(T(A))) \sqrt{N}(T_N(A) - T(A))$$

the variable  $\sqrt{N}(T_N(A) - T(A))$  converges to a Gaussian variable (since  $Z$  is a Gaussian process) with zero mean and variance is given by (7).

## References

- Adair RK (2003) Noise and stochastic resonance in voltage-gated ion channels. *Biosystems* 100(21):12099–12104
- Arhem P, Blomberg C (2007) Ion channel density and threshold dynamics of repetitive firing in a cortical neuron model. *Biosystems* 89(1–3):117–125
- Berry MJ, Warland DK, Meister M (1997) The structure and precision of retinal spike trains. *Proc Natl Acad Sci USA* 94:5411–5416
- Chase SM, Young ED (2008) Cues for sound localization are encoded in multiple aspects of spike trains in the inferior colliculus. *J Neurophysiol* 99:1672–1682
- Chen Y, Yu L, Qin SM (2008) Detection of subthreshold pulses in neurons with channel noise. *Phys Rev E* 78:51909
- Chow CC, White JA (1996) Spontaneous action potentials due to channel fluctuations. *Biophys J* 71(6):3013–3021
- Colbert CM, Johnston D (1996) Axonal action-potential initiation and Na<sup>+</sup> channel densities in the soma and axon initial segment of subicular pyramidal neurons. *J. Neurosci* 16(21):6676–6686
- Colbert CM, Pan P (2002) Ion channel properties underlying axonal action potential initiation in pyramidal neurons. *Nat Neurosci* 5(6):533–538
- Ethier SN, Kurtz TG (1986) Markov processes, characterization and convergence. John Wiley and Sons, Inc
- Furukawa S, Middlebrooks JC (2002) Cortical representation of auditory space: information-bearing features of spike patterns. *J Neurophysiol* 87:1749–1762
- Gillespie DT (1977) Exact stochastic simulation of coupled chemical reactions. *J Phys Chem* 81(25):2340–2361
- Gollisch T, Meister M (2008) Rapid neural coding in the retina with relative spike latencies. *Science* 319(1):1108–1111
- Guyonneau R, VanRullen R, Thorpe SJ (2005) Spike times make sense. *Trends Neurosci* 28(1):1–4
- Heil P (2004) First-spike latency of auditory neurons revisited. *Curr Opin Neurobiol* 14:461–467
- Hille B (2001) Ion channels of excitable membranes. Sinauer, Sunderland, MA
- Hodgkin AL (1948) The local electric changes associated with repetitive action in a non-medullated axon. *J Physiol* 107:165–181
- Izhikevich EM (2007) Dynamical systems in neuroscience: the geometry of excitability and bursting. In: Computational neuroscience. MIT Press
- Jenison RL, Reale RA (2003) Likelihood approaches to sensory coding in auditory cortex. *Netw Comput Neural Syst* 14:83–102
- Johansson RS, Birznieks I (2004) First spikes in ensembles of human tactile afferents code complex spatial fingertip events. *Nat Neurosci* 7:170–177
- Kiani R, Esteky H, Tanaka K (2005) Differences in onset latency of macaque inferotemporal neural responses to primate and non-primate faces. *J Neurophysiol* 94(2):1587–1596
- Kjaer TW, Gawne TJ, Richmond BJ (1996) Latency: another potential code for feature binding in striate cortex. *J Neurophysiol* 76(2):1356–1360
- Krishna BS (2002) A unified mechanism for spontaneous-rate and first-spike timing in the auditory nerve. *J Comput Neurosci* 13:71–91
- Lansky P, Musila M (1991) Variable initial depolarization in Stein's neuronal model with synaptic reversal potentials. *Biol Cybern* 64:285–291
- Lieberman MC (1978) Auditory-nerve response from cats raised in a low-noise chamber. *J Acoust Soc Am* 63(2):442–455
- Manns D, Westecker ME (1983) Antidromic activation of spikes with bimodal and trimodal latencies in the olfactory bulb of rabbits. *Brain Res* 288(1–2):119–130
- Mormann F, Kornblith S, Quiñero R, Kraskov A, Cerf M, Fried I, Koch C (2008) Latency and selectivity of single neurons indicate hierarchical processing in the human medial temporal lobe. *J Neurosci* 28(36):8865–8872
- Morris C, Lecar H (1981) Voltage oscillations in the barnacle giant muscle fiber. *Biophys J* 35(1):193–213
- Oser M, Uzuntarla M (2008) Effects of the network structure and coupling strength on the noise-induced response delay of a neuronal network. *Phys Lett A* 372:4603–4609
- Pakdaman K, Thieullen M, Wainrib G (2009) Fluid limit theorems for stochastic hybrid systems with application to neuron models. *J Appl Probab* (accepted)
- Pankratova EV, Polovinkin AV, Mosekilde E (2005) Resonant activation in a stochastic Hodgkin-Huxley model: Interplay between noise and suprathreshold driving effects. *Eur Phys J B* 45:391–397
- Panzeri S, Petersen RS, Schultz SR, Lebedev M, Diamond ME (2001) The role of spike timing in the coding of stimulus location in rat somatosensory cortex. *Neuron* 29:769–777
- Reulen JPH (1984) Latency of visually evoked saccadic eye movements. *Biol Cybern* 50(4):251–262
- Rinzel J, Ermentrout GB (1989) Analysis of neural excitability and oscillations. In: Methods in neuronal modeling: from synapses to networks, MIT Press, Cambridge, MA, pp 135–169
- Rowat P (2007) Interspike interval statistics in the stochastic Hodgkin-Huxley model: coexistence of gamma frequency bursts and highly irregular firing. *Neural Comput* 19(5):1215
- Ruggero MA (1992) Physiology and coding of sound in the auditory nerve. In: Popper AN, Fay RR (eds) The mammalian auditory pathway. Springer-Verlag, New York, NY, pp 34–93
- Schneidman E, Freedman B, Segev I (1998) Ion channel stochasticity may be critical in determining the reliability and precision of spike timing. *Neural Comput* 10(7):1679–1703
- Shuai JW, Jung P (2003) Optimal ion channel clustering for intracellular calcium signaling. *Proc Natl Acad Sci* 100(2):506–512
- Skaugen E, Walloe L (1979) Firing behavior in a stochastic nerve membrane model based upon the Hodgkin-Huxley equations. *Acta Physiol Scand* 107(4):343–363
- Tanabe S, Pakdaman K (2001) Noise-induced transitions in excitable neuron models. *Biol Cybern* 85:269–280
- Thorpe S, Fize D, Marlot C (1996) Speed of processing in the human visual system. *Nature* 381(6582):520–522



- Tuckwell HC, Wan FYM (2005) Time to first spike in stochastic Hodgkin-Huxley systems. *Physica A* 351(2–4):427–438
- van Rossum MCW (2001) The transient precision of integrate and fire neurons: effect of background activity and noise. *J Comput Neurosci* 10:303–311
- van Rossum MCW, O'Brien BJ, Smith RG (2003) Effects of noise on the spike timing precision of retinal ganglion cells. *J Neurophysiol* 89:2406–2419
- Van Rullen R (2003) Visual saliency and spike timing in the ventral visual pathway. *J Physiol Paris* 97(2-3):365–377
- Verveen AA, Derksen HE (1965) Fluctuations in membrane potential of axons and the problem of coding. *Biol Cybern* 2(4):153–160
- Wollner DA, Catterall WA (1986) Localization of sodium channels in axon hillocks and initial segments of retinal ganglion cells. *Proc Natl Acad Sci USA* 83(21):8424–8428